

## Dichroic Two-Photon Rubidium Frequency Standard

C. Perrella<sup>1,\*</sup>, P.S. Light,<sup>1</sup> J.D. Anstie,<sup>1,2,3</sup> F.N. Baynes,<sup>1</sup> R.T. White<sup>1</sup>, and A.N. Luiten<sup>1</sup>

<sup>1</sup>*Institute for Photonics and Advanced Sensing and School of Physical Sciences, The University of Adelaide, Adelaide, Australia*

<sup>2</sup>*BRITELab, Harry Perkins Institute of Medical Research, Queen Elizabeth II Medical Centre, Nedlands, Australia*

<sup>3</sup>*Centre for Medical Research, The University of Western Australia, Perth, Australia*



(Received 5 July 2019; published 27 November 2019)

We demonstrate an optical frequency standard based on the  $5S_{1/2} \rightarrow 5D_{5/2}$  two-photon transition of rubidium. The transition is interrogated in a Doppler-free arrangement by two lasers at 780 and 776 nm, with the sum frequency of the two lasers locked to the two-photon transition. We measure the fractional frequency stability of the frequency standard to be  $1.5 \times 10^{-13}$  at 1 s, reaching  $4.9 \times 10^{-14}$  at approximately 100 s, by comparison with an optical frequency comb. Performance limitations are presented and a clear pathway to an order-of-magnitude improvement is discussed. This platform has the potential to deliver a compact, robust standard for commercial and industrial applications.

DOI: 10.1103/PhysRevApplied.12.054063

### I. INTRODUCTION

Atomic frequency standards can be split into two broad domains. The first is ultrahigh-stability frequency standards based on laser-cooled atoms and ions, which can reach a fractional frequency stability of  $10^{-18}$  [1–5]. These high-stability devices have been used for tests of general relativity [3,6–9], investigation of the temporal stability of fundamental constants [3,10–13], and exploration of atomic physics [3,14–18]. The second domain is compact atomic frequency standards aimed at commercial and industrial markets, where fractional frequency stabilities in the range from  $10^{-10}$  to  $10^{-13}$  are desired. These devices, based on either optical [19–24] or microwave [25–29] atomic transitions, are aimed at, for example, telecommunications [25] or navigational [30] applications. Here we aim to bridge the gap between these two domains by building a standard that demonstrates a frequency stability similar to the very-best commercial frequency standards (e.g., the hydrogen maser, with a fractional frequency stability of approximately  $10^{-13}$  at an integration time of 1 s) while exhibiting the compactness and robustness of a portable standard. We propose to achieve this by exploiting the energy-level structure of rubidium (Rb) to efficiently drive a narrow-linewidth two-photon transition.

Previous work has shown the Rb  $5S_{1/2} \rightarrow 5D_{5/2}$  two-photon transition to be a promising candidate for a high-stability frequency standard, with a frequency stability of  $3 \times 10^{-13}/\sqrt{\tau}$  for  $1 < \tau < 1000$  s being reached [31,32]. More recently an impressive long-term result was shown,

$4 \times 10^{-13}/\sqrt{\tau}$  for  $1 < \tau < 10000$  s, which reached a stability of  $4 \times 10^{-15}$  at  $\tau = 10000$  s [23]. These standards used a single laser in a Doppler-free excitation technique to produce a spectral linewidth,  $\gamma$ , of 334 kHz [33], limited solely by the lifetime of the  $5D_{5/2}$  state. These simple two-photon standards detect fluorescence from the  $5D$  level as a measure of the frequency detuning between the output of the standard and the exact two-photon transition frequency.

The ultimate stability limit for such a frequency standard is set by the spectral linewidth of the transition, and the photon shot noise in the detected fluorescence, resulting in a fractional frequency stability  $\sigma(\tau)$  proportional to  $\gamma / (\nu \sqrt{N\tau})$ , where  $\nu$  is the transition frequency,  $N$  is the detected fluorescence photon flux, and  $\tau$  is the measurement integration time [34]. In addition, the detected fluorescence flux,  $N$ , is proportional to the two-photon transition rate, which itself is proportional to  $I^2/(\gamma \Delta^2)$ , where  $I$  is the pump-laser intensity and  $\Delta$  represents the single-photon detuning from a fortuitous  $5P_{3/2}$  intermediate level that lies almost midway between the  $5S_{1/2}$  and  $5D_{5/2}$  levels [35]. We see that the performance of the standard is linearly dependent on the applied intensity and on this detuning. For a conventional frequency standard, which makes use of a single laser to drive the two-photon transition, the single-photon detuning of  $\Delta \approx 1.1$  THz leads to a relatively low two-photon rate, and hence one typically compensates with increased intensity through optical cavities [31,32] or high-power driving lasers (tens of milliwatts) [23]. These approaches lead to better frequency stability at the cost of high power consumption and/or complexity and fragility.

\* chris.perrella@adelaide.edu.au

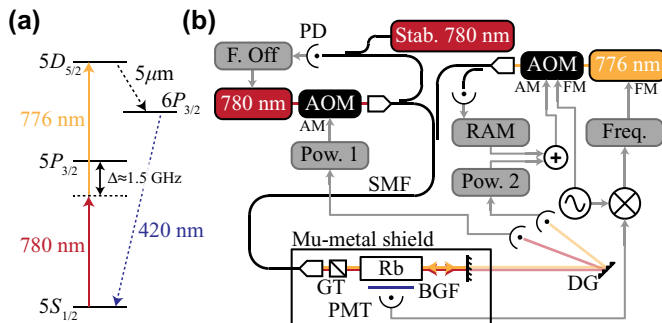


FIG. 1. (a) Two-photon-transition energy-level diagram. Solid arrows are driving excitations and dashed arrows show decay routes. (b) The experimental setup. The lasers are 780- and 776-nm extended-cavity diode lasers (ECDLs) and a 780-nm laser stabilized to Rb. AM, amplitude modulation; AOM, acousto-optic modulator; BGF, blue-glass filters; DG, diffraction grating; F. Off, frequency-offset lock for the 780 nm ECDL; FM, frequency modulation; Freq., frequency stabilization for the 776-nm ECDL; GT, Glan-Taylor polarizer; PD, photodiode; Pow. 1, power stabilization for the 780-nm ECDL; Pow. 2, power stabilization for the 776-nm ECDL; RAM, residual-amplitude-modulation cancellation; Rb, rubidium cell; SMF, single-mode fiber.

The innovation presented here uses dichroic excitation to more effectively exploit the intermediate atomic energy level. We do this by using a two-color excitation technique to drive the  $^{87}\text{Rb } 5S_{1/2}(F=2) \rightarrow 5D_{5/2}(F=4)$  transition as shown in Fig. 1(a). The use of two colors allows us to tune the intermediate-state detuning  $\Delta$  arbitrarily, greatly increasing the two-photon transition rate. Unfortunately this comes at the cost of introducing a small residual Doppler sensitivity. In the work reported here, we reduce the intermediate-state detuning  $\Delta$  to 1.5 GHz, which broadens the transition linewidth,  $\gamma$ , by a factor of approximately 8, but overall increases the two-photon transition rate by a factor of approximately  $10^5$  when compared with single-color Rb two-photon standards [23, 31, 32]. The increase in transition rate corresponds to a 25-fold improvement in the ultimate frequency stability for the same incident power. This is the key benefit of this approach as it allows a significant decrease in laser powers, which can lead to a simpler standard while maintaining high performance. It is important to note that with this approach it is the sum frequency of the two lasers that is frequency locked to the two-photon transition and it is thus the sum frequency that is the stable output of the standard.

## II. EXPERIMENT

Two extended-cavity diode lasers at approximately 780 nm and approximately 776 nm drive the two-photon transition [see Fig. 1(a)] using the experimental setup shown in Fig. 1(b). The beams from both lasers are combined in a single-mode fiber for spatial mode filtering and to minimize optical alignment fluctuations. Before being

launched into the Rb cell, the polarization of both laser beams is filtered with a Glan-Taylor prism to ensure high polarization purity of the excitation light. Both laser beams are launched into the cell and retroreflected by a partially reflecting mirror to allow Doppler-free spectroscopy of the two-photon transition [36]. Within the Rb-vapor cell the laser beams have a  $1/e^2$ -intensity diameter of 1.5 mm and optical powers of  $P_{776} = 1.2$  mW and  $P_{780} = 0.75$  mW.

When the sum of the laser frequencies is in resonance with the two-photon transition, 420-nm fluorescence is produced from atomic decay through the  $6P_{3/2} \rightarrow 5S_{1/2}$  transition; see Fig. 1(a). This fluorescence is spectrally separated from scattered light of the pump lasers by blue-glass filters and monitored with a photomultiplier tube (PMT) on the side of the Rb cell. The Rb cell is heated to approximately 90 °C to increase the Rb density and hence the blue-fluorescence intensity. A mu-metal shield encases the PMT, the Rb cell, and its heater to reduce ambient magnetic fields.

A critical issue in two-photon frequency standards arises from frequency shifts induced by the pumping light (light shifts) [23, 37]. To generate a substantial two-photon-transition rate, the driving excitation light needs to be strong. When combined with relatively broad transitions, this leads to large light shifts in the two-photon-transition frequency. This necessitates tight control of the detuning and power of the exciting lasers. In this standard this is achieved with three control loops: power stabilization of both the 776-nm laser and the 780-nm laser, and frequency stabilization of the 780-nm laser. Two additional control loops stabilize the frequency of the 776-nm laser and remove residual amplitude modulation (RAM) from the 776-nm light.

Stabilization of the laser powers interacting with the Rb vapor is achieved by our monitoring a small fraction (approximately 3%) of the light that is transmitted through the retroreflection mirror. A diffraction grating separates the 776- and 780-nm beams, which are detected on separate photodiodes. The detected power of each laser is stabilized by feeding correction signals back to their respective acousto-optic modulators.

The magnitude of the light shifts scales with detuning from the intermediate state, and thus  $\Delta$  needs to be stabilized to minimize the unwanted light shifts. This is achieved by our stabilizing the 780-nm laser's detuning from the  $5S_{1/2} \rightarrow 5P_{3/2}$  state using an offset lock to an auxiliary laser that had been locked to the  $5S_{1/2} \rightarrow 5P_{3/2}$  transition, indicated by “Stab. 780 nm” in Fig. 1(b).

Once the 780-nm laser has been frequency stabilized, we stabilize the sum of the two laser frequencies onto the two-photon resonance by controlling the frequency of the 776-nm laser. We generate an appropriate error signal, proportional to the difference frequency between the sum laser frequency and two-photon resonance, by frequency modulating the 776-nm beam using an acousto-optic modulator

at 660 kHz with a modulation depth of 2.5 MHz. This results in a synchronous population modulation of the  $5D_{5/2}$  state, and hence also the 420-nm fluorescence. The amplitude-modulated 420-nm fluorescence detected by the PMT is amplified and demodulated to produce a frequency discriminator centered at the two-photon-transition frequency as shown in the upper part of Fig. 2. The 776-nm-laser frequency is actively locked to the zero crossing of the frequency discriminator signal, as marked in Fig. 2. The control-loop bandwidth is approximately 100 kHz, limited by the relatively low modulation frequency used.

A second concern for residual instability beyond light shifts is unwanted RAM at the modulation frequency of the 776-nm laser, generated as a by-product of the frequency modulation. This RAM creates a false error signal that shifts the sum frequency of the two lasers to be off the exact two-photon resonance. Furthermore, any fluctuation in the RAM leads to an overall frequency instability in the optical atomic reference. To suppress these effects, the phase and amplitude of the RAM are detected and then fed back into the power control of the 776-nm laser with the opposite phase, canceling the RAM contribution.

For use as a compact frequency standard, the stable optical sum frequency at approximately 389 nm could be generated by mixing the two lasers in a nonlinear crystal. However, in this demonstration a commercial fiber optical frequency comb is used to create a virtual sum-frequency output. The two lasers (at frequencies  $f_{776}$  and  $f_{780}$ ) are mixed with the respective closest optical modes (numbered  $n_1$  and  $n_2$ ) of the frequency comb, generating beat notes at  $(f_{776} - f_{n1})$  and  $(f_{780} - f_{n2})$ , respectively, which are recorded with synchronously triggered counters. The frequency of the  $n$ th mode can be expressed as  $f_n = nf_{RR} + f_0$  where  $f_{RR}$  is the repetition rate of the comb and  $f_0$  is the

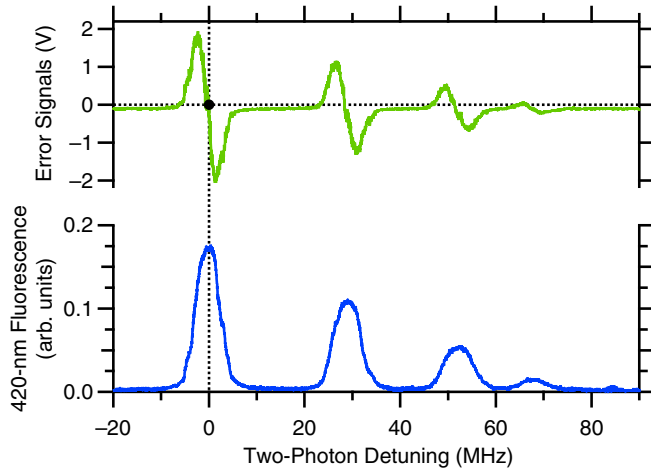


FIG. 2. Bottom: PMT-detected 420-nm fluorescence from atomic decay through the  $6P_{3/2} \rightarrow 5S_{1/2}$  transition. Multiple peaks arise from the  $5D_{5/2}$  hyperfine splitting. Top: Frequency discriminator used to lock the sum frequency of the two lasers to the two-photon transition.

carrier-envelope offset frequency [38]. In postprocessing, the two mixing products are mixed together to produce a new signal at frequency  $(f_{776} - f_{n1}) + (f_{780} - f_{n2}) = f_{776} + f_{780} - (n_1 + n_2)f_{RR} - 2f_0$ . In our measurement  $f_0$  is stabilized to a Cs-beam clock with a residual instability at the submillihertz level; thus, the instability introduced by this term is negligible when compared with that of the optical frequency standard. This new doubly mixed signal has the same frequency fluctuations as the “virtual” output signal but has a carrier frequency of 150 MHz.

### III. RESULTS

The two-photon-fluorescence signal produces a Voigt profile with a full width at half maximum of  $3.6 \pm 0.3$  MHz. This is substantially larger than the natural linewidth of 667 kHz [33], predominantly due to a calculated  $3.09 \pm 0.02$  MHz of residual Doppler broadening at the Rb-vapor temperature, due to the different wavelengths of the exciting lasers [36]. Convolution of the Doppler and natural linewidths gives an estimated full width at half maximum of  $3.47 \pm 0.02$  MHz, in agreement with the observed value.

Figure 3 presents the fractional frequency stability of the sum-frequency output of the standard when stabilized to the two-photon transition. A fractional frequency stability of  $1.5 \times 10^{-13}$  is measured at an integration time of 1 s, which averages down to  $4.9 \times 10^{-14}$  at an integration time of approximately 60 s. This is achieved by our balancing the noise contributions from light-shift fluctuations, shot

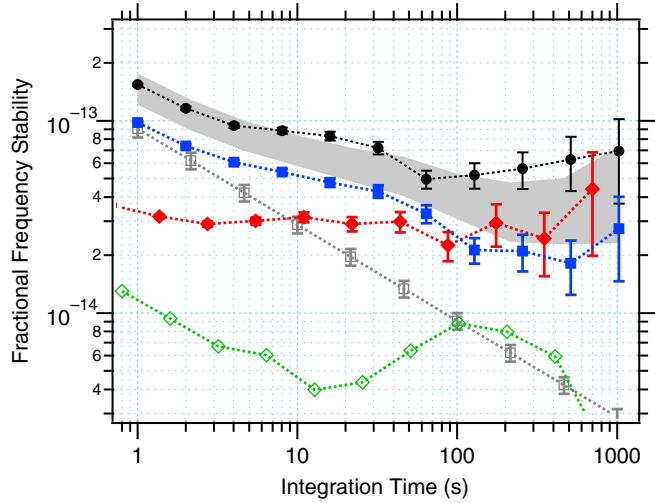


FIG. 3. Fractional frequency stability of the sum frequency when the lasers are stabilized (black circles). Also shown are the major noise sources in the standard, including light shifts (blue squares), photon shot noise (gray open squares), and the electronic noise floor (red diamonds). The sum of the noise sources is shown by the gray shaded region. The frequency stability of the optical frequency comb that measures the stability of the frequency standard is also shown (open green diamonds).

noise and electronics noise by tuning the optical powers driving the two-photon transition. The measured noise floors for these noise sources are shown in Fig. 3 and are summarized along with other relevant noise sources in Table I.

Under typical experimental conditions ( $I_{776} = 680 \text{ W/m}^2$  and  $I_{780} = 420 \text{ W/m}^2$ ), the theoretically expected light shifts are  $54 \pm 1 \text{ kHz}$  and  $315 \pm 1 \text{ kHz}$  for the 776- and 780-nm beams, respectively [39,40]. The measured light shifts are within a factor of 2 of the theoretically expected values [39,40]. These light shifts induce frequency noise through optical power fluctuations, which is one of the main limitations to frequency stability over all integration times measured (see Fig. 3). At integration time  $\tau = 1 \text{ s}$ , the fractional power stability for the 776- and 780-nm lasers is  $1 \times 10^{-3}$  and  $9 \times 10^{-5}$ , respectively, which generates light-shift-induced frequency instabilities of  $3.2 \times 10^{-14}$  and  $7.9 \times 10^{-14}$ , respectively.

Effective light shifts also arise from any frequency fluctuations of the individual lasers that change the detuning from the  $5P_{3/2}$  intermediate state and scale the magnitude of the light shifts. At a detuning of 1.5 GHz from the intermediate state, the light shifts vary by  $-170 \text{ Hz/MHz}$  [40]. As the 780-nm laser is offset locked to a stabilized laser, the fluctuation in detuning from the intermediate state is 11 kHz at integration time  $\tau = 1 \text{ s}$ . This corresponds to an instability of  $2.2 \times 10^{-15}$  at  $\tau = 1 \text{ s}$ , well below the measured stability.

An additional noise contribution is associated with shot noise of the 420-nm-fluorescence detection. Under typical operation, the PMT generates 0.44 nA of photocurrent from the detected 50 nW of 420-nm fluorescence. The small photocurrent is limited by the collection efficiency of approximately 0.2% and the low quantum efficiency of the PMT (approximately 8%) at this wavelength. The

TABLE I. Stability limits and frequency shifts of the dichroic two-photon Rb frequency standard. A description of each is found in the main text.

Physical effect	Fractional frequency stability at $\tau = 1 \text{ s}$	Frequency shift
<b>Light shifts</b>		
776-nm power	$3.2 \times 10^{-14}$	$54 \pm 1 \text{ kHz}$
780 nm power	$7.9 \times 10^{-14}$	$-315 \pm 1 \text{ kHz}$
$5P_{3/2}$ detuning	$2.2 \times 10^{-15}$	...
Shot noise	$9.1 \times 10^{-14}$	...
Electronic noise	$3.2 \times 10^{-14}$	$<70 \text{ kHz}$
RIN	$5.1 \times 10^{-14}$	...
PMT dark noise	$1.8 \times 10^{-15}$	...
RAM	$1.5 \times 10^{-15}$	...
Rb-Rb collisions	$<1 \times 10^{-15}$	$-1.82 \pm 0.01 \text{ kHz}$
Magnetic field	$<1 \times 10^{-15}$	$<1.5 \text{ kHz}$
Blackbody-radiation shift	$<2 \times 10^{-18}$	$-210 \text{ Hz}$

effect of the shot noise on the stability is estimated to be  $9.1 \times 10^{-14}/\sqrt{\tau}$ .

The final major contribution to the frequency instability is electronic noise in the feedback loop. The effect of electronic noise is estimated by monitoring the frequency-discriminator noise when the lasers are tuned out of resonance with the two-photon transition. These fluctuations correspond to a fractional frequency stability of  $3.2 \times 10^{-14}$  at  $\tau = 1 \text{ s}$  and are attributed to thermal sensitivity of the electronic components present in the feedback loop.

Other potential noise sources are listed in Table I but do not contribute significantly to instability at the current level of performance. Here we provide further description of each of these noise sources. The relative intensity noise (RIN) of the lasers at frequencies near the modulation frequency produces fictitious error signals after demodulation. This noise is additive and thus sets a limit to the minimum resolvable frequency fluctuations. Both the 776-nm laser and the 780-nm laser have a RIN of  $10^{-6}/\sqrt{\text{Hz}}$  around the modulation frequency, which translates into a noise floor with a fractional frequency stability of  $5.1 \times 10^{-14}/\sqrt{\tau}$ . The dark noise of the PMT is raised above its specified value as it is operating at an elevated temperature due to its close proximity to the heated Rb cell. Even so, the PMT dark current leads to a white frequency noise floor of  $1.8 \times 10^{-15}/\sqrt{\tau}$ , substantially below the current measured stability. RAM that was not suppressed by active feedback leads to a false error signal, a noise contribution of  $1.5 \times 10^{-15}$  at integration time  $\tau = 1 \text{ s}$ . The Rb cell is heated to approximately  $90^\circ\text{C}$  to increase the Rb density; however, this also increases Rb-Rb collisions, which produce a frequency shift of  $-1.82 \pm 0.01 \text{ kHz}$  [23,31]. Residual temperature fluctuations at the millikelvin level also have an influence on the long-term stability but can be estimated to be below the  $10^{-15}$  level [31,42,43]. The high temperature of the Rb cell generates only a small blackbody-radiation shift of approximately  $-210 \text{ Hz}$ , with a sensitivity of  $1 \text{ Hz/K}$  [31,41]. A mu-metal shield reduces ambient magnetic fields to  $2.0 \pm 0.5 \text{ mG}$  with a noise of  $0.01 \text{ mG}$  over  $100 \text{ s}$ . The associated frequency shift and noise are at the level of less than  $1.5 \text{ kHz}$  and less than  $10^{-15}$ , respectively, for  $\tau < 100 \text{ s}$ .

#### IV. DISCUSSION

Substantial improvements to the stability of this frequency standard can be gained by increasing the stability of the optical powers interacting with the Rb vapor and the signal-to-noise ratio of the frequency discriminator. The power stability of each laser can be increased significantly, to below  $1 \times 10^{-5}$  for  $1 < \tau < 10000 \text{ s}$ , with careful design of the power-control system [44]. This would reduce the light-shift frequency-noise contribution to below  $10^{-14}$  for  $1 < \tau < 10000 \text{ s}$ . Careful tuning of

the optical powers of the 776- and 780-nm lasers could additionally cancel the frequency offset generated by the light shift of each laser [37]. Furthermore, recent progress using Ramsey-based interrogation protocols that make use of composite laser-pulse sequences has shown promise in elimination of light shifts [45–47].

Increasing the fraction of collected fluorescence from approximately 0.2% to 5% and the PMT quantum efficiency from 8% to 50% leads to an increase in detected signal by a factor of approximately 160, reducing the shot-noise contribution by approximately 10 times to  $7 \times 10^{-15}$ , and the electronic-noise floor by approximately 160 times to  $6 \times 10^{-16}$ . This would push the frequency stability to the mid- $10^{-14}$  range at  $\tau = 1$  s, allowing this compact platform to compete in performance with the much-larger and more-expensive hydrogen maser.

Further improvements to the stability of the frequency standard could be made by utilizing frequency-doubled fiber lasers to drive the two-photon transition [23]. This would reduce the frequency instabilities generated by the laser's RIN to a frequency contribution below  $10^{-15}$ , leading to a frequency standard capable of performing in the  $10^{-15}$  regime for  $\tau > 100$  s.

## V. CONCLUSION

We demonstrate an optical frequency standard based on a two-color excitation of a two-photon Doppler-free transition in Rb. The standard exhibits a fractional frequency stability of  $1.5 \times 10^{-13}$  at an integration time of 1 s, and this reaches  $4.9 \times 10^{-14}$  at approximately 100 s. This result is competitive with previously published Rb two-photon frequency standards [23,31,32]. The current performance limits are identified as a combination of light shifts, photon shot noise, and electronic noise. There are well-known techniques to improve these limits, and we expect that by implementation of such changes this platform can offer a route to a fractional frequency stability of  $10^{-14}$  at an integration time of 1 s. Hence, the architecture demonstrated here can potentially deliver hydrogen-maser performance but in a frequency standard of a few liters in volume.

## ACKNOWLEDGMENTS

The authors acknowledge financial support from the Australian Research Council under Grants No. DP0877938, No. DE120102028, and No. FT0991631. This research is supported by the South Australian Government through the Premier's Science and Research Fund. This work is covered by U.S. patent application US20180329274A1.

[1] N. Hinkley, J. A. Sherman, N. B. Phillips, M. Schioppo, N. D. Lemke, K. Belyo, M. Pizzocaro, C. W. Oates, and A.

D. Ludlow, An atomic clock with  $10^{-18}$  instability, *Science* **341**, 1215 (2013).

- [2] T. L. Nicholson, S. L. Campbell, R. B. Hutson, G. E. Marti, B. J. Bloom, R. L. McNally, W. Zhang, M. D. Barrett, M. S. Safronova, G. F. Strouse, W. L. Tew, and J. Ye, Systematic evaluation of an atomic clock at  $2 \times 10^{-18}$  total uncertainty, *Nat. Commun.* **6**, 6896 (2015).
- [3] A. D. Ludlow, M. M. Boyd, J. Ye, E. Peik, and P. O. Schmidt, Optical atomic clocks, *Rev. Mod. Phys.* **87**, 637 (2015).
- [4] S. Origlia, M. S. Pramod, S. Schiller, Y. Singh, K. Bongs, R. Schwarz, A. Al-Masoudi, S. Dörscher, S. Herbers, S. Häfner, U. Sterr, and Ch. Lisdat, Towards an optical clock for space: Compact, high-performance optical lattice clock based on bosonic atoms, *Phys. Rev. A* **98**, 053443 (2018).
- [5] W. F. McGrew, X. Zhang, R. J. Fasano, S. A. Schäffer, K. Belyo, D. Nicolodi, R. C. Brown, N. Hinkley, G. Milani, M. Schioppo, T. H. Yoon, and A. D. Ludlow, Atomic clock performance enabling geodesy below the centimetre level, *Nature* **564**, 87 (2018).
- [6] S. Reinhardt, G. Saathoff, H. Buhr, L. A. Carlson, A. Wolf, D. Schwalm, S. Karpuk, C. Novotny, G. Huber, M. Zimmerman, R. Holzwarth, T. Udem, T. W. Hänsch, and G. Gwinner, Test of relativistic time dilation with fast optical atomic clocks at different velocities, *Nat. Phys.* **3**, 861 (2007).
- [7] C. W. Chou, D. B. Hume, T. Rosenband, and D. J. Wineland, Optical clocks and relativity, *Science (New York, N.Y.)* **329**, 1630 (2010).
- [8] P. Delva *et al.*, Test of Special Relativity Using a Fiber Network of Optical Clocks, *Phys. Rev. Lett.* **118**, 221102 (2017).
- [9] J. Grotti *et al.*, Geodesy and metrology with a transportable optical clock, *Nat. Phys.* **14**, 437 (2018).
- [10] S. Bize, S. A. Diddams, U. Tanaka, C. E. Tanner, W. H. Oskay, R. E. Drullinger, T. E. Parker, T. P. Heavner, S. R. Jefferts, L. Hollberg, W. M. Itano, and J. C. Bergquist, Testing the Stability of Fundamental Constants with the  $^{199}\text{Hg}^+$  Single-Ion Optical Clock, *Phys. Rev. Lett.* **90**, 150802 (2003).
- [11] T. Rosenband, D. B. Hume, P. O. Schmidt, C. W. Chou, A. Brusch, L. Lorini, W. H. Oskay, R. E. Drullinger, T. M. Fortier, J. E. Stalnaker, S. A. Diddams, W. C. Swann, N. R. Newbury, W. M. Itano, D. J. Wineland, and J. C. Bergquist, Frequency ratio of  $\text{Al}^+$  and  $\text{Hg}^+$  single-ion optical clocks; metrology at the 17th decimal place, *Science (New York, N.Y.)* **319**, 1808 (2008).
- [12] R. M. Godun, P. B. R. Nisbet-Jones, J. M. Jones, S. A. King, L. A. M. Johnson, H. S. Margolis, K. Szymaniec, S. N. Lea, K. Bongs, and P. Gill, Frequency Ratio of Two Optical Clock Transitions in  $^{171}\text{Yb}^+$  and Constraints on the Time Variation of Fundamental Constants, *Phys. Rev. Lett.* **113**, 210801 (2014).
- [13] N. Huntemann, B. Lipphardt, C. Tamm, V. Gerginov, S. Weyers, and E. Peik, Improved Limit on a Temporal Variation of  $m_p/m_e$  from Comparisons of  $\text{Yb}^+$  and  $\text{Cs}$  Atomic Clocks, *Phys. Rev. Lett.* **113**, 210802 (2014).
- [14] A. Brusch, R. Le Targat, X. Baillard, M. Fouché, and P. Lemonde, Hyperpolarizability Effects in a Sr Optical Lattice Clock, *Phys. Rev. Lett.* **96**, 103003 (2006).

- [15] H. Katori, Optical lattice clocks and quantum metrology, *Nat. Photonics* **5**, 203 (2011).
- [16] M. Bishop, M. J. Martin, M. D. Swallows, C. Benko, Y. Lin, G. Quéméner, A. M. Rey, and J. Ye, Inelastic collisions and density-dependent excitation suppression in a  $^{87}\text{Sr}$  optical lattice clock, *Phys. Rev. A* **84**, 052716 (2011).
- [17] A. Goban, R. B. Hutson, G. E. Marti, S. L. Campbell, M. A. Perlin, P. S. Julienne, J. P. D’Incao, A. M. Rey, and J. Ye, Emergence of multi-body interactions in a fermionic lattice clock, *Nature* **563**, 369 (2018).
- [18] M. A. Norcia, J. R. K. Cline, J. A. Muniz, J. M. Robinson, R. B. Hutson, A. Goban, G. E. Marti, J. Ye, and J. K. Thompson, Frequency Measurements of Superradiance from the Strontium Clock Transition, *Phys. Rev. X* **8**, 021036 (2018).
- [19] K. Knabe, S. Wu, J. Lim, K. A. Tillman, P. S. Light, N. Wheeler, F. County, R. Thapa, A. M. Jones, J. W. Nicholson, B. R. Washburn, F. Benabid, and K. L. Corwin, 10 kHz accuracy of an optical frequency reference based on  $^{12}\text{C}_2\text{H}_2$ -filled large-core kagome photonic crystal fibers, *Opt. Express* **17**, 16017 (2009).
- [20] A. Lurie, F. N. Baynes, J. D. Anstie, P. S. Light, F. Benabid, T. M. Stace, and A. N. Luiten, High-performance iodine fiber frequency standard, *Opt. Lett.* **36**, 4776 (2011).
- [21] P. S. Light, J. D. Anstie, F. Benabid, and A. N. Luiten, Hermetic optical-fiber iodine frequency standard, *Opt. Lett.* **40**, 2703 (2015).
- [22] M. T. Hummon, S. Kang, D. G. Bopp, Q. Li, D. A. Westly, S. Kim, C. Fredrick, S. A. Diddams, K. Srinivasan, V. Aksyuk, and J. E. Kitching, Photonic chip for laser stabilization to an atomic vapor with  $10^{-11}$  instability, *Optica* **5**, 443 (2018).
- [23] K. W. Martin, G. Phelps, N. D. Lemke, M. S. Bigelow, B. Stuhl, M. Wojcik, M. Holt, I. Coddington, M. W. Bishop, and J. H. Burke, Compact Optical Atomic Clock Based on a Two-Photon Transition in Rubidium, *Phys. Rev. Appl.* **9**, 014019 (2018).
- [24] Z. L. Newman *et al.*, Architecture for the photonic integration of an optical atomic clock, *Optica* **6**, 680 (2019).
- [25] S. Knappe, V. Shah, P. Schwindt, L. Hollberg, J. Kitching, L. Liew, and J. Moreland, A microfabricated atomic clock, *Appl. Phys. Lett.* **85**, 1460 (2004).
- [26] F.-X. Esnault, D. Holleville, N. Rossetto, S. Guerandel, and N. Dimarcq, High-stability compact atomic clock based on isotropic laser cooling, *Phys. Rev. A* **82**, 033436 (2010).
- [27] S. Micalizio, C. E. Calosso, A. Godone, and F. Levi, Metrological characterization of the pulsed Rb clock with optical detection, *Metrologia* **49**, 425 (2012).
- [28] S. Kang, M. Gharavipour, C. Affolderbach, F. Gruet, and G. Milet, Demonstration of a high-performance pulsed optically pumped Rb clock based on a compact magnetron-type microwave cavity, *J. Appl. Phys.* **117**, 104510 (2015).
- [29] M. Langlois, L. De Sarlo, D. Holleville, N. Dimarcq, J.-F. Schaff, and S. Bernon, Compact Cold-Atom Clock for Onboard Timebase: Tests in Reduced Gravity, *Phys. Rev. Appl.* **10**, 064007 (2018).
- [30] F. Esnault, N. Rossetto, D. Holleville, J. Delporte, and N. Dimarcq, HORACE: A compact cold atom clock for Galileo, *Adv. Space Res.* **47**, 854 (2011).
- [31] L. Hilico, R. Felder, D. Touahri, O. Acef, A. Clairon, and F. Biraben, Metrological features of the rubidium two-photon standards of the BNM-LPTF and Kastler Brossel Laboratories, *Eur. Phys. J.: Appl. Phys.* **4**, 219 (1998).
- [32] Y. Milleroux, D. Touahri, L. Hilico, A. Clairon, R. Felder, F. Biraben, and B. Debeauvoir, Towards an accurate frequency standard at  $\lambda = 778$  nm using a laser diode stabilized on a hyperfine component of the Doppler-free two-photon transitions in rubidium, *Opt. Commun.* **108**, 91 (1994).
- [33] D. Sheng, A. Pérez Galván, and L. A. Orozco, Lifetime measurements of the  $5d$  states of rubidium, *Phys. Rev. A* **78**, 062506 (2008).
- [34] H. S. Margolis, Optical frequency standards and clocks, *Contemp. Phys.* **51**, 37 (2010).
- [35] C. Perrella, P. S. Light, J. D. Anstie, T. M. Stace, F. Benabid, and A. N. Luiten, High-resolution optical spectroscopy in a hollow-core photonic crystal fiber, *Phys. Rev. A* **87**, 013818 (2013).
- [36] J. Bjorkholm and P. Liao, Line shape and strength of two-photon absorption in an atomic vapor with a resonant or nearly resonant intermediate state, *Phys. Rev. A* **14**, 751 (1976).
- [37] V. Gerginov and K. Beloy, Two-Photon Optical Frequency Reference with Active ac Stark Shift Cancellation, *Phys. Rev. Appl.* **10**, 014031 (2018).
- [38] S. T. Cundiff and J. Ye, Colloquium: Femtosecond optical frequency combs, *Rev. Mod. Phys.* **75**, 325 (2003).
- [39] S. C. Rand, *Lectures on Light: Nonlinear and Quantum Optics Using the Density Matrix* (Oxford University Press, Oxford, 2010).
- [40] P. F. Liao and J. E. Bjorkholm, Direct Observation of Atomic Energy Level Shifts in Two-Photon Absorption, *Phys. Rev. Lett.* **34**, 1 (1975).
- [41] J. W. Farley and W. H. Wing, Accurate calculation of dynamic Stark shifts and depopulation rates of Rydberg energy levels induced by blackbody radiation. Hydrogen, helium, and alkali-metal atoms, *Phys. Rev. A* **23**, 2397 (1981).
- [42] K. Weber and K. Niemax, Self-broadening and shift of Doppler-free two-photon lines of Rb, *Opt. Commun.* **31**, 52 (1979).
- [43] B. P. Stoicheff and E. Weinberger, Frequency Shifts, Line Broadenings, and Phase-Interference Effects in  $\text{Rb}^* + \text{Rb}$  Collisions, Measured by Doppler-Free Two-Photon Spectroscopy, *Phys. Rev. Lett.* **44**, 733 (1980).
- [44] F. Tricot, D. H. Phung, M. Lours, S. Guérandel, and E. de Clercq, Power stabilization of a diode laser with an acousto-optic modulator, *Rev. Sci. Instrum.* **89**, 113112 (2018).
- [45] V. I. Yudin, A. V. Taichenachev, M. Yu. Basalaev, T. Zanon-Willette, J. W. Pollock, M. Shuker, E. A. Donley, and J. Kitching, Generalized Autobalanced Ramsey Spectroscopy of Clock Transitions, *Phys. Rev. Appl.* **9**, 054034 (2018).
- [46] C. Sanner, N. Huntemann, R. Lange, C. Tamm, and E. Peik, Autobalanced Ramsey Spectroscopy, *Phys. Rev. Lett.* **120**, 53602 (2018).
- [47] M. Shuker, J. W. Pollock, R. Boudot, V. I. Yudin, A. V. Taichenachev, J. Kitching, and E. A. Donley, Ramsey Spectroscopy with Displaced Frequency Jumps, *Phys. Rev. Lett.* **122**, 113601 (2019).